

**MAXIMUM POWER POINT TRACKING USING  
LLC RESONANT CONVERTER FOR PV POWER  
SYSTEMS**

**ADRIAN TAN SOON THEAM**

**UNIVERSITI SAINS MALAYSIA**

**2016**

**MAXIMUM POWER POINT TRACKING USING LLC  
RESONANT CONVERTER FOR PV POWER SYSTEMS**

**by**

**ADRIAN TAN SOON THEAM**

**Thesis submitted in fulfilment of the requirements  
for the degree of  
Master of Science**

**May 2016**

## **ACKNOWLEDGEMENTS**

Life is a journey and along the way, we get to meet great people that helped make us a better person. I am truly fortunate to meet some great people in my journey here in USM.

First and foremost, I would like to extend my greatest gratitude to Dr. Shahid Iqbal for your guidance and patience. I am extremely lucky to have a good mentor and a friend like you. Thank you for your advice and mentorship on my projects as well as on how to be a good researcher.

To my parents and Debra, thank you for your support and love. Whenever I am lost, I could always count on my family to guide me back on the right path. Words of encouragement and quality family time go a long way especially in the life of research.

Next, to my lab mates and postgraduate friends especially Hong Ye, Wei Jun, Leong, Nick, Faisal, Azura and Imran, thank you for your friendship. I enjoy having discussion and sharing laughter together with you guys.

Finally, I would like to express my gratitude to staffs and technicians of School of Electrical and Electronics Engineering for their help in making studying in USM a truly wonderful experience.

# TABLE OF CONTENTS

	Page
Acknowledgements.....	ii
Table of Contents .....	iii
List of Tables .....	vii
List of Figures .....	viii
List of Plates .....	xii
List of Abbreviations .....	xiii
List of Symbols .....	xiv
Abstrak.....	xviii
Abstract .....	xix
CHAPTER 1 – INTRODUCTION	
1.1 Introduction .....	1
1.2 Problem Statement .....	5
1.3 Objectives .....	6
1.4 Project Scope .....	6
1.5 Thesis Outline .....	8
CHAPTER 2 – LITERATURE REVIEW	
2.1 Introduction .....	9
2.2 Photovoltaic Cell .....	9
2.3 Maximum Power Point Tracking (MPPT) .....	15
2.4 DC-DC Converters for MPPT .....	16
2.4.1 PWM DC-DC Converters.....	17
2.4.1.1 Buck Converter.....	17
2.4.1.2 Boost Converter .....	19

2.4.1.3	Buck-Boost Converter .....	20
2.4.1.4	Cuk Converter .....	22
2.4.1.5	SEPIC .....	23
2.4.2	Resonant Converters .....	24
2.4.2.1	Series Resonant Converter .....	25
2.4.2.2	Parallel Resonant Converter .....	29
2.4.2.3	Series-Parallel Resonant Converter .....	31
2.4.2.4	LLC Resonant Converter .....	34
2.5	Comparisons of DC-DC Converters .....	37
2.6	MPPT Algorithms .....	39
2.6.1	Differentiation Method .....	40
2.6.2	Feedback Voltage/Current Method .....	41
2.6.3	Perturb and Observe (P&O) Technique .....	42
2.6.4	Incremental Conductance Technique .....	43
2.6.5	Forced Oscillation Technique .....	45
2.6.6	Artificial Intelligence Methods .....	45
2.7	Comparisons of MPPT Methods .....	46
2.8	Battery Charging Characteristics .....	48
 CHAPTER 3 – METHODOLOGY		
3.1	Introduction .....	50
3.2	LLC Resonant Converter Based MPPT System .....	50
3.3	LLC Resonant Converter .....	51
3.3.1	Operation of LLC Resonant Converter .....	51
3.3.2	Gain Analysis of LLC resonant converter .....	57
3.4	INC Algorithm for LLC resonant converter .....	62
3.5	INC Algorithm with Constant Voltage Control .....	66

## CHAPTER 4 – DESIGN AND IMPLEMENTATION

4.1	Introduction .....	72
4.2	PV Module Characteristics.....	72
4.3	Design and Implementation of LLC Resonant Converter .....	75
4.3.1	Initial Design Parameters .....	75
4.3.2	Transformer Turn Ratio, $n$ .....	77
4.3.3	Gain of LLC Resonant Converter .....	78
4.3.4	Equivalent Load Resistance, $R_{eq}$ .....	78
4.3.5	Quality Factor, $Q$ and Inductance Ratio, $L_n$ .....	79
4.3.6	Resonant Capacitance, $C_r$ , Resonant Inductance, $L_r$ and Magnetizing Inductance, $L_m$ .....	80
4.3.7	Structure of Power Transformer .....	81
4.4	Implementation of INC MPPT Controller with CV Mode .....	81
4.4.1	Voltage Sensor .....	82
4.4.2	Current Sensor .....	84
4.4.3	Measurement Averaging Algorithm.....	85
4.4.4	Switching Signal Generation Algorithm .....	86
4.4.5	Incremental Conductance Algorithm.....	87
4.4.6	Constant Voltage Mode .....	89

## CHAPTER 5 – RESULTS AND DISCUSSIONS

5.1	Introduction .....	91
5.2	Simulation of LLC Resonant Converter with INC MPPT .....	91
5.3	Prototype and Experimental Verification .....	94
5.3.1	MPPT Waveforms.....	95
5.3.1.1	Case A: Progress of MPPT when INC Algorithm is Activated.....	95

5.3.1.2	Case B: Progress of MPPT during Sudden Drop of Irradiance .....	97
5.3.1.3	Case C: Progress of MPPT during Sudden Rise of Irradiance .....	98
5.3.2	Whole Day Operation with LLC Resonant Converter.....	100
5.3.3	Constant Voltage Charging .....	106
CHAPTER 6 – CONCLUSION		
6.1	Conclusion .....	110
6.2	Future work .....	110
References .....		111
LIST OF PUBLICATIONS .....		118
APPENDICES		
APPENDIX A – CIRCUIT SCHEMATICS AND LAYOUTS		

## LIST OF TABLES

		<b>Page</b>
Table 2.1	Comparisons of MPPT	47
Table 3.1	SOC estimation of 12V lead-acid battery	67
Table 4.1	SPM100-M PV Module Electrical Characteristics.	72
Table 5.1	Design Specifications	92



## LIST OF FIGURES

		Page
Figure 1.1	World energy consumption by fuel type, 1990-2040 (quadrillion Btu)	2
Figure 1.2	Solar PV total global capacity, 2004-2013	2
Figure 1.3	Solar PV capacity and additions, top 10 countries, 2013	3
Figure 1.4	The global PV module price learning curves for c-Si wafer-based and CdTe modules, 1979 to 2015	4
Figure 1.5	Configuration of PV generation system suitable for residential homes	5
Figure 2.1	Equivalent circuit of single-diode five-parameter model for a PV module	10
Figure 2.2	I-V characteristics of a PV module	13
Figure 2.3	P-V characteristics of a PV module	14
Figure 2.4	Block diagram of PV power generation system	15
Figure 2.5	Various operating point on the I-V curve	16
Figure 2.6	Buck converter circuit diagram	17
Figure 2.7	Operating and non-operating region of buck converter	18
Figure 2.8	Boost converter circuit diagram	19
Figure 2.9	Operating and non-operating region of boost converter	20
Figure 2.10	Buck-boost converter circuit diagram	20
Figure 2.11	Operating region of buck-boost converter	21
Figure 2.12	Cuk converter circuit diagram	22
Figure 2.13	SEPIC converter circuit diagram	23
Figure 2.14	Block diagram of a resonant converter	24
Figure 2.15	Full-bridge series resonant converter	26
Figure 2.16	AC equivalent circuit of SRC	26
Figure 2.17	DC gain characteristics of SRC	28

Figure 2.18	Full-bridge parallel resonant converter	29
Figure 2.19	AC equivalent circuit of PRC	29
Figure 2.20	DC gain characteristics of PRC	30
Figure 2.21	Full-bridge series-parallel resonant converter	32
Figure 2.22	AC equivalent circuit of SPRC	32
Figure 2.23	DC gain characteristics of SPRC	33
Figure 2.24	Full-bridge LLC series resonant converter	35
Figure 2.25	AC equivalent circuit of LLC resonant converter	35
Figure 2.26	DC gain characteristics of LLC	36
Figure 2.27	Block diagram of voltage-feedback technique	41
Figure 2.28	Perturb and observe tracking process	42
Figure 2.29	Different variations of $dP/dV$ for incremental conductance algorithm	44
Figure 2.30	Three-step lead-acid battery charging profile	49
Figure 3.1	Block diagram of proposed system	51
Figure 3.2	Circuit of LLC resonant converter	52
Figure 3.3	Key steady-state waveforms of LLC resonant converter	52
Figure 3.4	Operation modes of the LLC resonant converter	56
Figure 3.4(a)	Mode 1	56
Figure 3.4(b)	Mode 2	56
Figure 3.4(c)	Mode 3	56
Figure 3.4(d)	Mode 4	56
Figure 3.5	Model of LLC resonant converter using FHA	58
Figure 3.6	Plots of voltage gain function for different values of $Q$ and $L_n$	61
Figure 3.6(a)	$L_n = 1$	61
Figure 3.6(b)	$L_n = 5$	61
Figure 3.6(c)	$L_n = 10$	61

Figure 3.6(d)	$L_n = 20$	61
Figure 3.7	Three regions on the P-V characteristic curve	63
Figure 3.8	Load line on I-V characteristic curve	64
Figure 3.9	Gain of LLC resonant converter for $Q = 0.2$ and $L_n = 4$	64
Figure 3.10	Flowchart of proposed INC algorithm	65
Figure 3.11	MPPT at region near to open-circuit voltage of PV panel	67
Figure 3.12	Flowchart of proposed CV algorithm	69
Figure 3.13	First case of CV control	69
Figure 3.14	Second case of CV control	70
Figure 4.1	Model of SPM100-M by using Simulink	73
Figure 4.2	I-V curves of SPM100-M under different weather conditions	74
Figure 4.3	P-V curves of SPM100-M under different weather conditions	74
Figure 4.4	Circuit diagram of the LLC resonant converter	76
Figure 4.5	DC gain characteristics of LLC resonant converter using FHA	79
Figure 4.6	Winding structure of power transformer of LLC resonant converter	82
Figure 4.7	Circuit diagram of the INC MPPT controller setup	83
Figure 4.8	Voltage sensing circuit	84
Figure 4.9	Current sensing circuit	85
Figure 5.1	Simulink diagram of the proposed LLC resonant converter for MPPT	92
Figure 5.2	Simulation results of the LLC resonant converter with INC algorithm	93
Figure 5.2(a)	Irradiance Level	93
Figure 5.2(b)	PV panel voltage	93
Figure 5.2(c)	PV panel current	93
Figure 5.2(d)	PV panel power	93

Figure 5.2(e)	Switching frequency	93
Figure 5.2(f)	Resonant current	93
Figure 5.3	The progress of MPPT when the INC algorithm is activated at $640\text{W/m}^2$ irradiance and $100\text{kHz}$ resonant switching frequency	95
Figure 5.4	The displacement of operating power points during tracking progress for case A	96
Figure 5.5	The progress of MPPT during sudden drop of irradiance from $754\text{W/m}^2$ to $310\text{W/m}^2$	97
Figure 5.6	The displacement of operating power points during tracking progress for case B	98
Figure 5.7	The progress of MPPT during sudden rise of irradiance of $310\text{W/m}^2$ to $754\text{W/m}^2$	99
Figure 5.8	The displacement of operating power points during tracking progress for case C	99
Figure 5.9	Experimental results for tracking the maximum power for one day	101
Figure 5.10	LLC resonant converter circuit with measured experimental parameters	102
Figure 5.11	Experimental waveforms at point $P_1$ : Primary-side bridge voltage, $v_{ab}$ , resonant inductor current, $i_{Lr}$ , secondary-side bridge voltage, $v_{cd}$ and secondary-side current, $i_s$ at irradiance of $206\text{W/m}^2$ with corresponding maximum power of $18.5\text{W}$	103
Figure 5.12	Experimental waveforms at point $P_2$ : Primary-side bridge voltage, $v_{ab}$ , resonant inductor current, $i_{Lr}$ , secondary-side bridge voltage, $v_{cd}$ and secondary-side current, $i_s$ at irradiance of $350\text{W/m}^2$ with corresponding maximum power of $36.5\text{W}$	104
Figure 5.13	Experimental waveforms at point $P_3$ : Primary-side bridge voltage, $v_{ab}$ , resonant inductor current, $i_{Lr}$ , secondary-side bridge voltage, $v_{cd}$ and secondary-side current, $i_s$ at irradiance of $724\text{W/m}^2$ with corresponding maximum power of $47.8\text{W}$	105
Figure 5.14	Efficiency of the converter as a function of input voltage	105
Figure 5.15	Efficiency of the converter as a function of input power	106
Figure 5.16	Irradiance and PV panel's power with CV mode for one day	108
Figure 5.17	Battery's voltage with CV mode for one day	109

## LIST OF PLATES

		<b>Page</b>
Plate 4.1	Photograph of experimental LLC resonant converter setup	76
Plate 4.2	Photograph of experimental INC MPPT controller setup	83
Plate 5.1	Experimental setup of implemented system	94

## LIST OF ABBREVIATIONS

<b>AC</b>	Alternating Current
<b>BESS</b>	Battery Energy Storage System
<b>CC</b>	Constant Current
<b>CV</b>	Constant Voltage
<b>DC</b>	Direct Current
<b>EMI</b>	Electromagnetic Interference
<b>FHA</b>	First Harmonic Approximation
<b>INC</b>	Incremental Conductance
<b>LLC-SRC</b>	LLC Series Resonant Converter
<b>MPP</b>	Maximum Power Point
<b>MPPT</b>	Maximum Power Point Tracking
<b>OECD</b>	Organization for Economic Cooperation and Development
<b>P&amp;O</b>	Perturb and Observe
<b>PV</b>	Photovoltaic
<b>PRC</b>	Parallel Resonant Converter
<b>PWM</b>	Pulse-Width Modulation
<b>RMS</b>	Root Mean Square
<b>SEPIC</b>	Single-Ended Primary Inductor Converter
<b>SOC</b>	State of Charge
<b>SPS</b>	Simulink-to-Physical Signal
<b>SPRC</b>	Series-Parallel Resonant Converter
<b>SRC</b>	Series Resonant Converter
<b>ZCS</b>	Zero Current Switching
<b>ZVS</b>	Zero Voltage Switching

## LIST OF SYMBOLS

$A$	Ideality Factor of the Diode
$c$	Step Size
$C$	Capacitance
$C_{bat}$	Capacity of the Battery in Ahr
$C_p$	Parallel Capacitance
$C_s$	Series Capacitance
$D$	Duty Cycle
$dI$	Change in Current
$dP$	Change in Power
$dV$	Change in Voltage
$dt$	Change in Time
$\Delta d$	Small Change in Duty Cycle
$\Delta V$	Small Change in Voltage
$e$	Permissible Error
$E$	Fundamental Input Voltage
$E_g$	Band Gap Energy
$f_n$	Normalized Frequency
$f_p$	Pole Resonant Frequency
$f_r$	Resonant Frequency
$f_s$	Switching Frequency
$G$	Solar Irradiation
$I$	PV Array Output Current
$I_d$	Cell Reverse Saturation Current
$i_{D1}$	Secondary-Side Diode Current
$I_{in}$	Input Current
$i_{Lr}$	Resonant Inductor Current
$i_{Lm}$	Magnetizing Inductor Current
$i_{Lm0}$	Magnetizing Inductor Current at time $t_0$

$I_{max}$	Maximum Charging Current
$I_{out}$	Output Current
$I_{ph}$	Cells Photo Current
$I_{p,f}$	Fundamental Primary Current
$I_{pv}$	PV Module Output Current
$I_{rr}$	Reverse Saturation Current at $T_r$
$I_{sc}$	Short-Circuit Current
$I_{scr}$	Cell Short Circuit Current
$I_{in,sense}$	PV Panel Sensing Current
$k$	Boltzmann's Constant
$k_i$	Short-Circuit Current Temperature Coefficient
$L$	Inductance
$L_r$	Resonant Inductance
$L_m$	Magnetizing Inductance
$L_n$	Inductance Ratio
$M$	DC Gain
$n$	Transformer Turn Ratio
$N_p$	Number of Modules Connected in Parallel
$N_s$	Number of Cells Connected in Series
$P$	PV Array Output Power
$P_{in,max}$	Maximum Input Power
$P_{MPP}$	Peak Power Point
$q$	Electron Charge
$Q$	Quality Factor
$R$	Resistance
$R_{eq}$	AC Equivalent Load Resistance
$R_{in}$	Input Resistance
$R_{in,fs2}$	Input Impedance at the Boundary between ZCS region and ZVS Region
$R_{in,fs1}$	Input Impedance at Region $dP/dV > 0$



$R_{in,fs2}$	Input Impedance at Region $dP/dV < 0$
$R_{MPP}$	Resistance at Maximum Power Point
$R_L$	Load Resistance
$R_o$	Output Resistance
$R_s$	Series Resistance
$R_{sh}$	Shunt Resistance
$T$	Cell Temperature
$t_{d,min}$	Minimum Dead Time
$T_r$	Cell Reference Temperature
$T_s$	Switching Period
$V$	PV Array Output Voltage
$v_{ab}$	Primary-Side Bridge Voltage
$V_{bat}$	Battery Voltage
$V_{bat,sense}$	Battery Sensing Voltage
$V_{bat,min}$	Minimum Battery Charging Voltage
$v_{cd}$	Secondary-Side Bridge Voltage
$v_{cr}$	Resonant Capacitor Voltage
$v_{cr0}$	Resonant Capacitor Voltage at time $t_0$
$V_d$	Voltage Drop of Output Diode
$v_{ds}$	Voltage across MOSFET
$V_{in}$	Input Voltage
$V_{in(max)}$	Maximum Input Voltage
$V_{in(min)}$	Minimum Input Voltage
$V_{in(nom)}$	Nominal Input Voltage
$V_{in,sense}$	PV Panel Sensing Voltage
$V_{max}$	Maximum Charging Voltage
$V_{MPP}$	Voltage at Maximum Power Point
$V_o$	Output Voltage
$V_{o,ac}$	AC Equivalent Output Voltage

$V_{oc}$	Open-Circuit Voltage
$V_{o(max)}$	Maximum Output Voltage
$V_{o(min)}$	Minimum Output Voltage
$V_{o(nom)}$	Nominal Output Voltage
$V_{p,f}$	Fundamental Primary Voltage
$V_{pv}$	PV Module Output Voltage
$V_{ref}$	Reference Voltage
$\omega_r$	Radian Frequency
$X$	Reactances

# **PENGESANAN TITIK KUASA MAKSIMUM DENGAN MENGGUNAKAN PENUKAR SALUNAN LLC UNTUK SISTEM KUASA PV**

## **ABSTRAK**

Pengesanan titik kuasa maksimum (MPPT) merupakan salah satu bahagian yang penting dalam pelbagai sistem fotovoltan (PV) dan telah dikaji dengan teliti dalam kajian lepas. Walau bagaimanapun, kebanyakan sistem pengesanan titik kuasa maksimum menggunakan penukar DC-DC permodulatan lebar denyut. Baru-baru ini, penukar salunan DC-DC menjadi terkenal untuk pemprosesan kuasa kerana mempunyai ciri-ciri yang baik seperti kehilangan pensuisan yang rendah, operasi frekuensi tinggi dan gangguan elektromagnetik yang rendah. Dalam penyelidikan ini, algoritma pengaliran tambahan (INC) dicadangkan dengan menggunakan penukar salunan LLC untuk pengesanan titik kuasa maksimum dalam sistem kuasa PV. Penukar salunan LLC mampu mengesan kuasa maksimum semasa beroperasi dengan pensuisan sifar voltan mengakibatkan kecekapan yang tinggi untuk operasi frekuensi tinggi. Selain itu, INC MPPT dengan mod voltan malar (CV) untuk pengecasan bateri dicadangkan dalam kajian ini. Pelaksanaan terperinci MPPT dengan mod CV algoritma dan carta aliran serta prosedur reka bentuk penukar dibincangkan dengan teliti dalam tesis ini. Keputusan eksperimen prototaip 100W menunjukkan bahawa penukar mencatat kecekapan puncak setinggi 81% untuk keseluruhan julat reka bentuk. Sebagai tambahan, penukar juga mempamerkan prestasi yang baik dalam menguasai kuasa maksimum di bawah pelbagai keadaan persekitaran sambil menonjolkan keupayaan pensuisan lancar.

# **MAXIMUM POWER POINT TRACKING USING LLC RESONANT CONVERTER FOR PV POWER SYSTEMS**

## **ABSTRACT**

Maximum power point tracking (MPPT) is a crucial part in any photovoltaic (PV) systems and is thoroughly addressed in the literature. However, most of the existing MPPT systems use pulse-width modulated DC-DC converters. Recently, resonant DC-DC converters have become famous for power processing due to their good characteristics such as low switching loss, high frequency operation and low electromagnetic interference. In this research work, an incremental conductance (INC) MPPT using LLC resonant converter is proposed for PV power systems. The LLC resonant converter can track the maximum power while operating in zero voltage switching region resulting in high efficiency for high frequency operation. In addition, an INC MPPT with constant voltage (CV) mode for battery charging is proposed in this study. Detailed implementation of the MPPT with CV mode algorithm and its flowchart as well as the design procedure of the LLC resonant converter is thoroughly discussed in this thesis. The experimental results of a 100W prototype shows that the converter obtains a peak efficiency of 81% for the entire design range. In addition, the converter exhibits good performance in capturing the maximum power under various environmental conditions while performing soft-switching capabilities.

# **CHAPTER 1**

## **INTRODUCTION**

### **1.1 Introduction**

Presently, the world energy is still predominantly generated by fossil fuel. Liquid fuel, coal and natural gas are the main sources of energy as shown in Figure 1.1. However, the world experiences severe global warming and climate change due to the extensive burning of fossil fuels for power generation in order to meet the growth of the world energy demand. The main cause of global warming is the emission of greenhouse gases, and the primary source of these gases is from fossil fuel burning (Committee on the Science of Climate Change of National Research Council, 2001; Oreskes, 2004). Furthermore fossil fuels are non-renewable resources. So it would be difficult to meet its ongoing demand (Owen, Inderwildi, & King, 2010). As a result of the said environmental issues, more researches are being pursued by related organizations for more efficient and green power generations. Renewable energies such as solar photovoltaic (PV), wind, wave, biomass and etc. are of great interest in research. The renewable energies are clean, inexhaustible and does not release greenhouse gases (Committee on the Science of Climate Change of National Research Council, 2001; Oreskes, 2004).

Over the past ten years, renewable energy has seen rapid technology advances and increasing deployment throughout the whole world. By adopting and shifting to renewable energy, we can reduce greenhouse emission and meet the increasing world energy demand. Furthermore, renewable energy helps mitigate future extreme weather

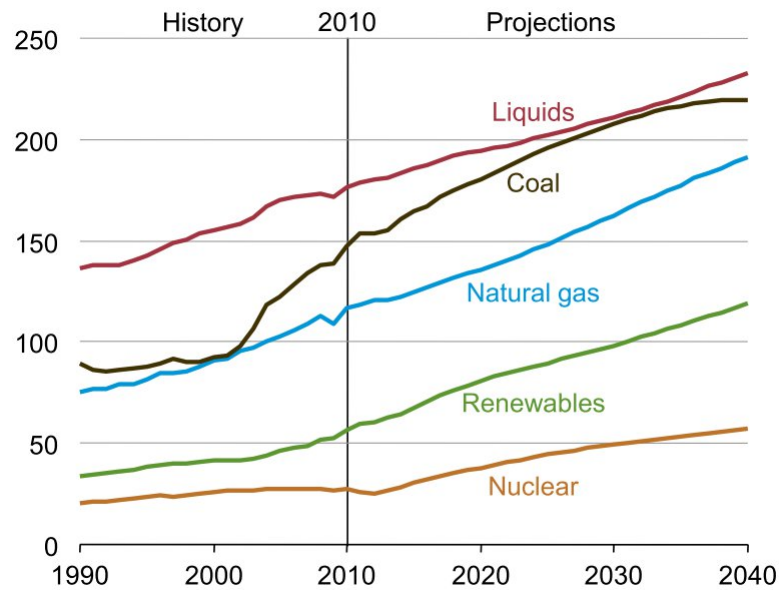


Figure 1.1: World energy consumption by fuel type, 1990-2040 (quadrillion Btu) (U.S. Energy Information Agency, 2013)

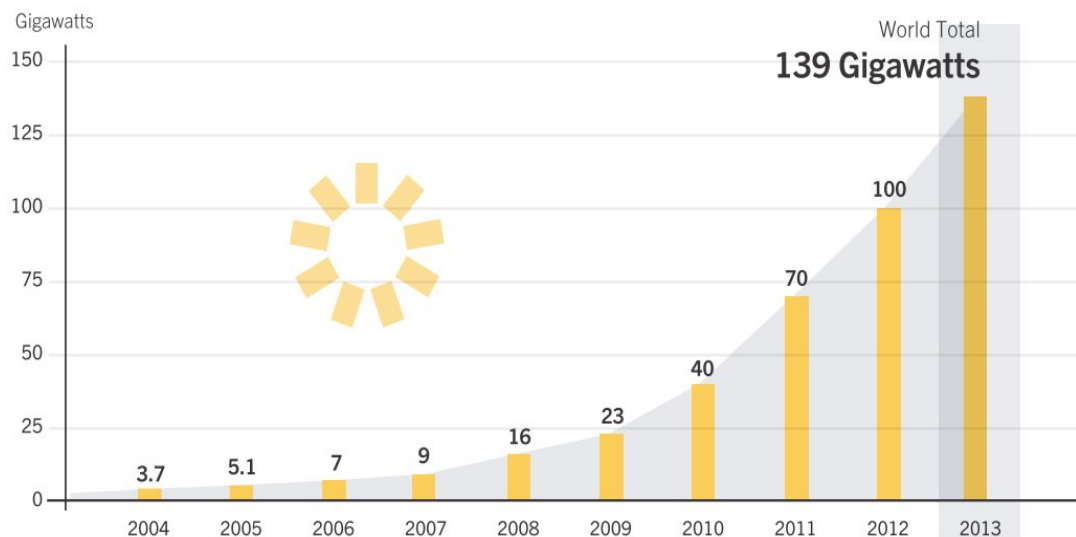


Figure 1.2: Solar PV total global capacity, 2004-2013 (Brower et al., 2014)

and climate changes. Through technological advances, timely and cost-efficient delivery of energy can be achieved (Ellabban, Abu-Rub, & Blaabjerg, 2014). In 2013, for the first time, new solar PV power capacity added surpassed the new wind power capacity added. Solar PV has continued to expand at a enormous rate, with a growth in global capacity averaging almost 55% annually over the past five years. In 2013, the world total solar capacity is at 139 GW as shown in Figure 1.2. From Figure 1.3,

China added the most PV capacity followed by Japan and United States (Brower et al., 2014).

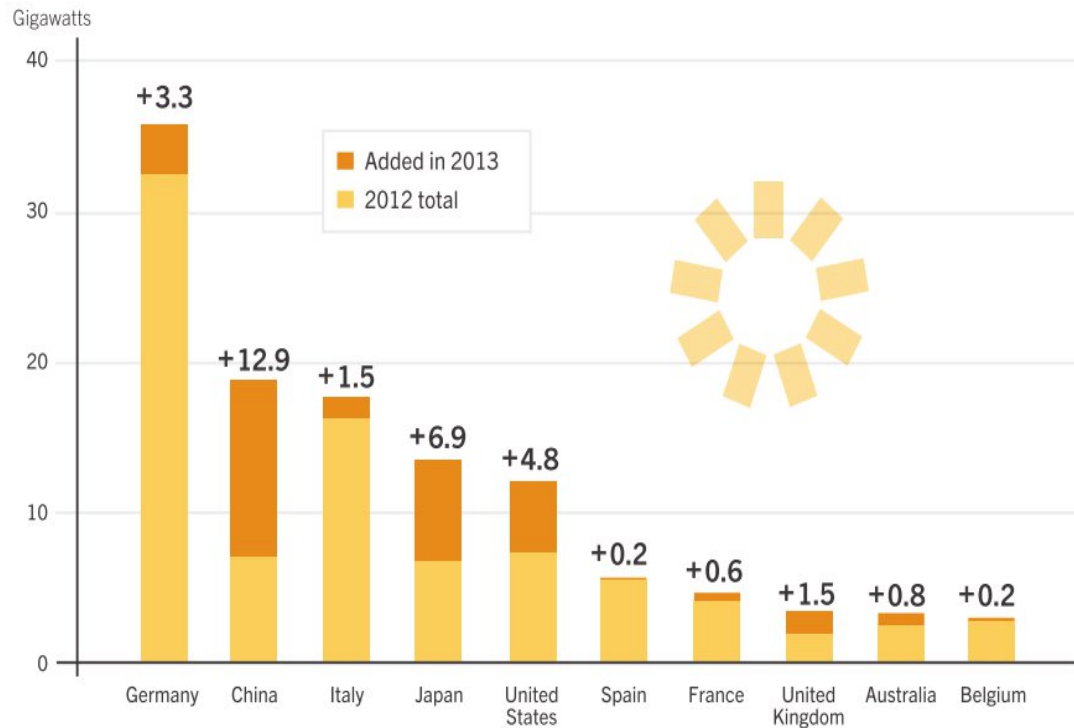


Figure 1.3: Solar PV capacity and additions, top 10 countries, 2013 (Brower et al., 2014)

Policy support from over 50 countries have been available for PV adoption and expansion such as PV feed-in tariffs (Hoppmann, Huenteler, & Girod, 2014; Zhi, Sun, Li, Xu, & Su, 2014). However the recent significant increase of PV usage is mainly due to rapid cost reductions of the PV as well as latest technology advancements that overcame some of the limitations that PV previously had. Conventional silicon cell (c-Si) modules are the most expensive PV technology, but they have the highest commercial efficiency. The global price for c-Si modules from 2004 to Q3 2008 is hovering around \$3.50-\$4.00/W. In 2009, facing steep price-point competition from thin-film (CdTe, CIG/CIGS) solar module, the price of c-Si modules dropped rapidly to \$2.00/W and still manufacturers are able to make positive operating margin (Bazilian et al.,

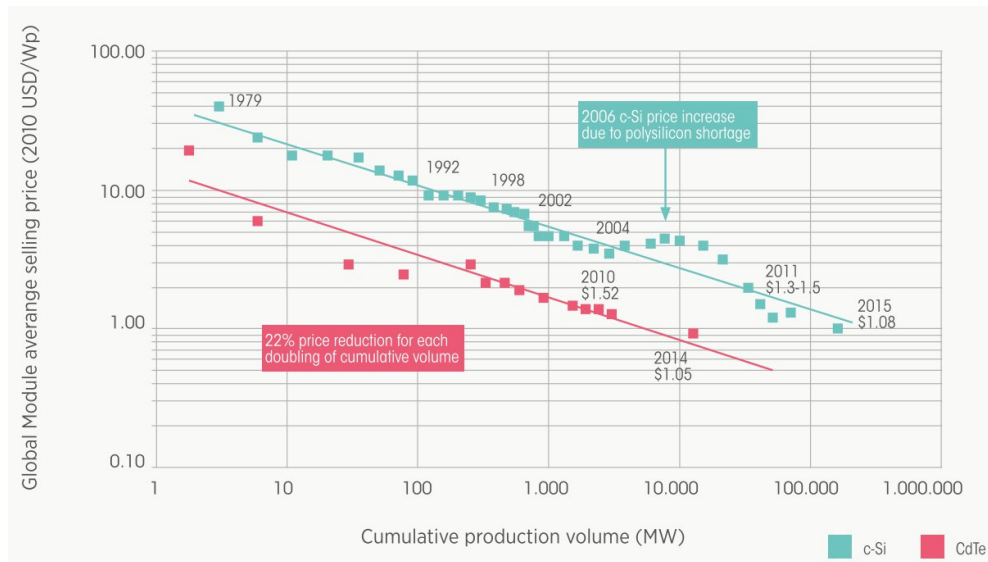


Figure 1.4: The global PV module price learning curves for c-Si wafer-based and CdTe modules, 1979 to 2015 (Agency, 2012)

2013). This success was due to the reductions in costs achieved over the past four years from technology advances and growing scale of production in wafer, cell and module manufacturing processes. Improved performance resulting from better cell efficiencies and lower electrical conversion losses also help in driving the cost down. In April 2012, c-Si PV modules fell below \$1.00/W. In March 2012, thin film module price ranges between \$0.79/W for Cds/CdTe to \$0.92/W for a-Si/ $\mu$ -Si modules (Bazilian et al., 2013). Top Chinese producers are fast approaching costs of \$0.50/W for c-Si modules in 2013 (Brower et al., 2014), clearly outperform the projected price done by International Renewable Energy Agency in June 2012 shown in Figure 1.4 (Agency, 2012). With the affordable price of PV modules, solar energy has the potential to be a great contributor in fulfilling the world energy demand and reducing greenhouse gases emission.

A basic block diagram of a PV power generation system suitable for residential homes is shown in Figure 1.5 (Mutoh et al., 2006). It consists of a PV array, a DC-DC